

Damage characterization of beam-column joints reinforced with GFRP under reversed cyclic loading

A. M. Said*

Dept. of Civil & Environmental Engineering, University of Nevada, Las Vegas, NV 89154, U.S.A.

(Received September 20, 2008, Accepted October 17, 2008)

Abstract. The use of fiber reinforced polymer (FRP) reinforcement in concrete structures has been on the rise due to its advantages over conventional steel reinforcement such as corrosion. Reinforcing steel corrosion has been the primary cause of deterioration of reinforced concrete (RC) structures, resulting in tremendous annual repair costs. One application of FRP reinforcement to be further explored is its use in RC frames. Nonetheless, due to FRP's inherently elastic behavior, FRP-reinforced (FRP-RC) members exhibit low ductility and energy dissipation as well as different damage mechanisms. Furthermore, current design standards for FRP-RC structures do not address seismic design in which the beam-column joint is a key issue. During an earthquake, the safety of beam-column joints is essential to the whole structure integrity. Thus, research is needed to gain better understanding of the behavior of FRP-RC structures and their damage mechanisms under seismic loading. In this study, two full-scale beam-column joint specimens reinforced with steel and GFRP configurations were tested under quasi-static loading. The control steel-reinforced specimen was detailed according to current design code provisions. The GFRP-RC specimen was detailed in a similar scheme. The damage in the two specimens is characterized to compare their performance under simulated seismic loading

Keywords: beam-column joint; frames; GFRP; grid; damage mechanics; NEFMAC; seismic.

1. Introduction

Steel reinforcement corrosion has been the primary cause of deterioration of RC structures, resulting in substantial annual repair costs worldwide. Additionally, various modern equipments that utilize magnetic interferometers (e.g. hospitals), require a nonmagnetic environment with non-metallic reinforcement. Consequently, fiber-reinforced polymers (FRP) reinforcement has been increasingly adopted in construction due to its nonmagnetic and corrosion resistance (Sugita 1993). Another major advantage of FRP reinforcement is the ease of embedding fiber optic strain measurement devices for structural health monitoring purposes. This ability can eventually introduce monitoring systems that mimic nervous systems in living organisms with the capacity to monitor loading and damage in real time.

A significant number of studies investigated the use of FRP reinforcement in flexural members (Nagasaka, *et al.* 1993, Alsayed, *et al.* 1997, Shehata 1999). For columns, Sharbatdar and Saatcioglu (2004) studied the behavior of carbon FRP-RC columns under simulated earthquake loading. They reported that specimens designed according to the CSA S806-02 (2002) can achieve drift capacities of 2-3%. They concluded that FRP-RC members may be designed to remain elastic during seismic

*Corresponding Author, E-mail: asaid@egr.unlv.edu

loading and that confinement can significantly improve the behavior of compression members. It was also noted that the grid structure can facilitate construction and provide a near-uniform distribution of confinement pressure along the column, without congesting the reinforcement cage.

Fukuyama, *et al.* (1995) tested a half-scale three-storey aramid FRP-RC frame, under quasi-static loading. It was argued that frame deformations governed the design. The frame remained elastic up to a drift angle of 2%. Limited damage in the form of beam longitudinal reinforcement rupture occurred at 4.4% drift with no substantial decrease in strength, owing to the high degree of structural indeterminacy of the frame. The frame performance satisfied the target design deformation for serviceability and ultimate limit states. It was also noted that the rehabilitation of such a frame was easier than that of conventional RC frames since residual deformations were smaller. The study acknowledged the feasibility of FRP-RC structures in seismic zones. This was later verified by Kobayashi, *et al.* (2003) and a design procedure for FRP-RC frames based on the Architectural Institute of Japan (AIJ) design guidelines was also outlined. The investigation concluded that FRP-RC structures may possibly be designed in seismic zones if the response is kept within the capacity of the FRP rebars. However, the study recommended the use of vibration control devices to enhance the damping of such structures.

Most of the newly adopted specifications for the design of FRP-reinforced concrete (440.1R-06 2006, CSA S806-02 2002, ISIS Canada 2001, JSCE 1997 and CHBDC 1998) are continuously updating and trying to cover more design aspects and to incorporate new research findings. These specifications are yet to include detailed seismic provisions. Accordingly, research is needed to investigate the performance of FRP-RC frames under reversed cyclic loading. This will help future design code provisions for FRP-RC in seismic zones. In this study, full-scale steel-reinforced and steel-free GFRP-RC beam-column joints were tested. Their damage under reversed cyclic loading is characterized to compare their performance.

The type of FRP grid used in this study is a GFRP NEFMAC (*New Fiber Composite Material for Reinforcing Concrete*). Typical stirrups (three-branched) used in this investigation were made out of GFRP NEFMAC grids in the form of four-cell units. These grids are also used in a wide range of applications such as bridge decks, barrier and curtain walls, water tanks, slabs-on-grade, underground tunnel linings, and rock storage cavities (Sugita 1993). The advantages of FRP grids include high durability and fatigue resistance (Rahman, *et al.* 2000), suppression of delamination problems, equal longitudinal and transverse reinforcement depth, and built-in redundancy (Dutta, *et al.* 1998).

2. Experimental program

Beam-column joints can be isolated from plane frames at the points of contraflexure. The column of the current test specimen is taken from the points of mid-height of two storeys, while the beam is considered at the point mid-span of the bay.

2.1. Steel-reinforced specimen (J1)

The first specimen in this study (Fig. 1) is a standard beam-column joint (J1) designed to satisfy both ACI 352R-02 (2002) and CSA A23.3-04 (2005) requirements. It has sufficient shear reinforcement in the joint area, in the column hinging area, and in the beam hinging area. The selected load history consisted of two phases. The first one was load-controlled up to yield, followed by a displacement-controlled phase.

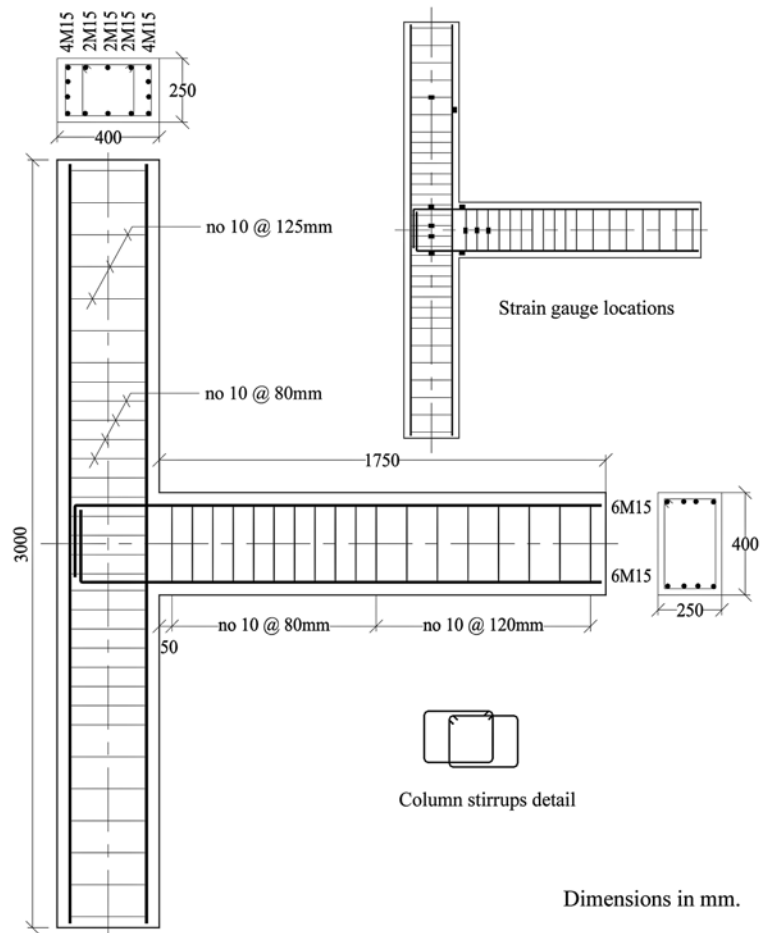


Fig. 1 Details of the standard steel-reinforced specimen (*J1*)

2.2. GFRP-reinforced specimen (*J4*)

The second beam-column joint specimen in this study (*J4*), shown in Fig. 2, had identical dimensions to specimen (*J1*) but was made with GFRP grid reinforcement and a slightly different reinforcement configuration. A view of the GFRP reinforcement cage is shown in Fig. 3. The use of 3 branched grid-shaped stirrups provides a built-in redundancy since the failure of a branch is not complete until both of its two vertical portions fail. Some properties of the NEFMAC grids are listed in Table 1. The choice of GFRP NEFMAC was based on the fact of its capacity to deform 1.67 times more than CFRP NEFMAC, thus giving a better indication of imminent failure owing to larger ultimate deformations. For this specimen, a displacement-controlled load history similar to the one adopted by Fukuyama, *et al.* (1995) was selected.

The assembly of the steel-free GFRP-RC (*J4*) specimens was performed at a much faster pace than that of the steel-reinforced specimen (*J1*). The stirrups, being taken from a manufactured grid, were dimensionally identical, thus, the longitudinal reinforcement needed very little rearrangement. The much lighter weight of the GFRP rebars allowed easier manipulation of the reinforcement cage. For the

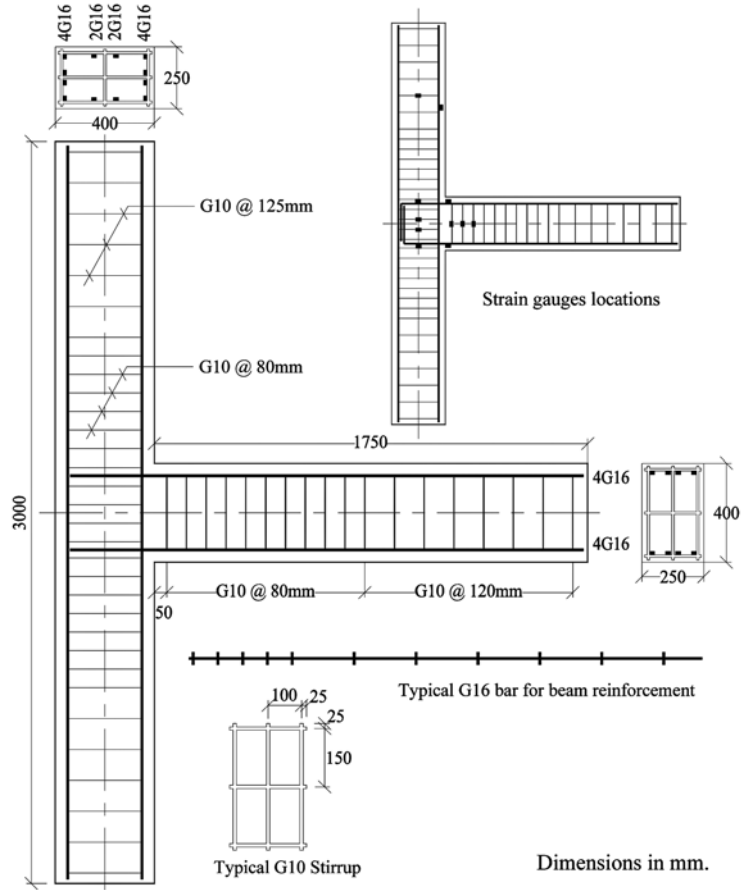


Fig. 2 Details of the GFRP-RC specimen (J4)



Fig. 3 View of the GFRP reinforcement cage for specimen (J4)

steel-reinforced specimen (J1), extra work was required to fit steel rebars in place, especially in the congested joint area where the steel stirrups configuration was more complicated.

Table 1 Properties of GFRP NEFMAC grids (NEFCOM 1996)

Bar Type and No.	Sectional Area (mm ²)	Max Load (kN)	Tensile Strength (MPa)	Modulus of Elasticity (GPa)
NEFMAC G10	77	46.7	600	30
NEFMAC G16	201	119.2	600	30

3. Results and analysis

For the two studied specimens, several parameters were used to evaluate performance and characterize damage sustained throughout the loading history.

3.1. Behavior of steel-reinforced specimen (J1)

The beam tip load-storey drift angle plot for the standard steel-reinforced specimen is shown in Fig. 4. Flexural cracking of the beam section at column face appeared at a beam tip load of 15 kN at 0.17% drift. The onset of diagonal cracks in the joint area took place at a beam tip load of 50 kN and a 0.6% drift. Afterwards, further cracking took place in the joint but remained within a very fine width throughout the test. The yield of beam’s longitudinal steel was reached at an average beam tip load of 107 kN and an average yield displacement, δ_y of 28 mm (1.50% drift). At a deformation level equal to $2\delta_y$ (3.0% drift), the flexural hinge formed at column face with a width equivalent to beam’s depth. At a deformation equal to $4\delta_y$ (6.0% drift), wide cracks developed in the hinge area of the beam and rubble started falling. At $6\delta_y$ (9.0% drift), the flexural hinge area of the beam lost most of its concrete and the test was stopped. The column was able to sustain its axial load throughout the test and the joint area remained intact, except the presence of fine cracks. Fig. 5 shows the final crack pattern of the standard specimen (J1).

3.2. Behavior of GFRP-reinforced specimen (J4)

The beam tip load-storey drift plot for the GFRP-RC specimen is shown in Fig. 6. The first flexural crack at the beam bottom adjacent to the column face was detected at a beam tip load of about 10.5 kN and 0.10% drift. A residual deformation at beam-tip of 1.6 mm was observed after the two 0.25% drift

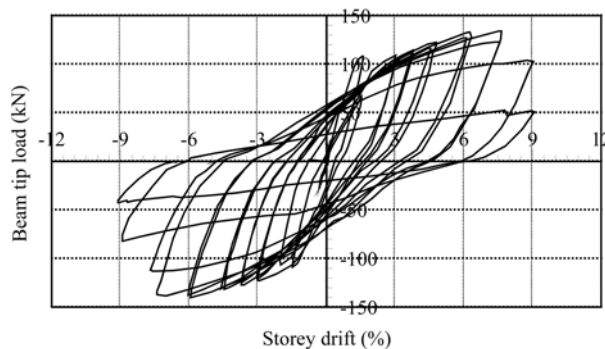


Fig. 4 Beam tip load-storey drift relationship for the standard steel-reinforced specimen J1



Fig. 5 Final crack pattern for the standard steel-reinforced specimen *J1*

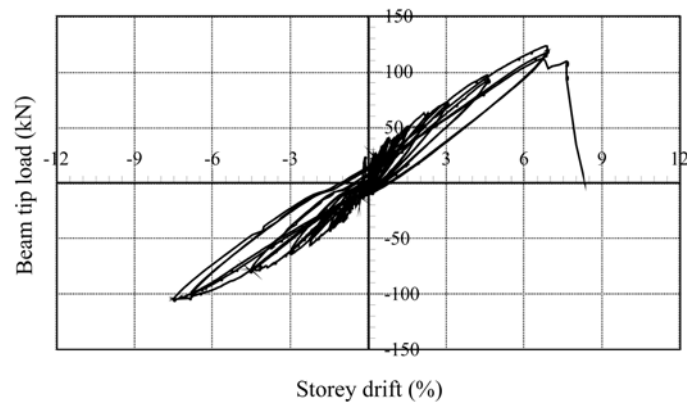


Fig. 6 Beam tip load-storey drift relationship for the GFRP-RC specimen *J4*

cycles. During further testing, several distinct cracks extended through the depth of the beam section at specific locations corresponding to grid nodes in the longitudinal reinforcement, while several smaller cracks formed along the beam. This took place since GFRP bars, which are originally cut from grids, are not deformed and the bond with concrete is predominantly supplied by the nodes. The onset of diagonal cracks in the joint area took place at a beam tip load of 42 kN during the 2% drift cycle. Additional cracks in the joint area appeared thereafter as loading progressed, but remained within a very fine width throughout the test. At 4.55% drift, excessive cracking have occurred in the beam and rubble started falling. Failure took place at the 5% drift angle in a sudden and brittle manner when two of the beam's bottom GFRP bars snapped in tension. The final crack pattern of the GFRP-RC specimen (*J4*) is shown in Fig. 7.

3.3. Load-storey drift angle envelope relationship

Fig. 8 shows the envelopes of the beam tip load-storey drift relationships for the tested specimens. Initially, the envelopes had comparable stiffness, but as soon as cracking took place a distinct difference

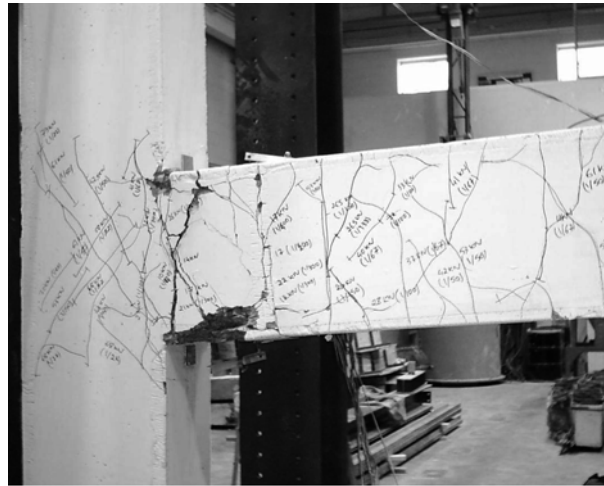


Fig. 7 Final crack pattern for the GFRP-RC specimen *J4*

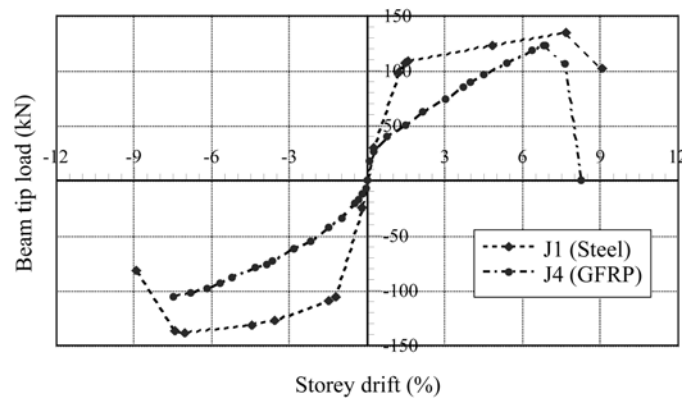


Fig. 8 Beam tip load-storey drift envelopes for the tested specimens

between the behavior of the specimens appeared and was significant for the remainder of the tests. The two envelopes indicate that specimens had comparable ultimate load capacity, but the GFRP-RC specimen exhibited lower stiffness, which is due to the lower stiffness of GFRP compared to that of steel. The GFRP-RC specimen (*J4*) had more than 10% lower total drift compared to that of the steel-reinforced (*J1*) specimen which had a stable post-yield load carrying capacity as expected. The GFRP-RC specimen (*J4*) had an essentially elastic envelope while the steel-reinforced specimen (*J1*) had a typical elastic-plastic envelope.

3.4. Storey shear-joint shear deformation relationship

The beam-column joint stiffness was monitored through the measurement of the joint panel deformation obtained using two LVDT's mounted diagonally across the corners of the joint area. The measured elongation and shortening of the joint diagonals versus load was used to derive the average joint shear deformation, which is equal to the sum of the horizontal and vertical shear deformation angles, denoted as γ_h and γ_v , respectively. The average shear deformation, $\gamma_{average}$, can be calculated as:

$$\gamma_{average} = \gamma_h + \gamma_v = \frac{\Delta_1 + \Delta_2}{D \sin 2\Phi} \tag{1}$$

where Δ_1 and Δ_2 are the elongation and shortening in the lengths of the diagonals, respectively, D is the length of the diagonal and Φ is the angle between the diagonal and the axis of the beam. The storey shear-joint deformation plots for specimens *J1* and *J4* are traced in Figs. 9 and 10, respectively. The storey shear, V_{actual} , was calculated taking into account the $P-\Delta$ effect based on work of Uzumeri and Seckin (1974) using the following equation:

$$V_{actual} = \frac{P\left(L/2 - \frac{\delta}{L/2}H\right) - N \times \frac{\delta}{L/2}H}{H} \tag{2}$$

where N is the column axial load, H is the column height, L is the beam’s length, and P and δ are the beam tip load and deformation, respectively.

Comparing the behavior of the two joint panels, it is clear that the steel-reinforced panel of specimen (*J1*) had higher stiffness and smaller joint deformation compared to that of the GFRP-RC panel. This produced higher joint contribution to the total deformation of the subassemblage in the case of the GFRP-RC specimen, which normally adds up to the lateral deformation of the frame. Fukuyama, *et al.* (1995) noticed that the measured lateral deformations for the 2 bay-3 storey half-scale AFRP-

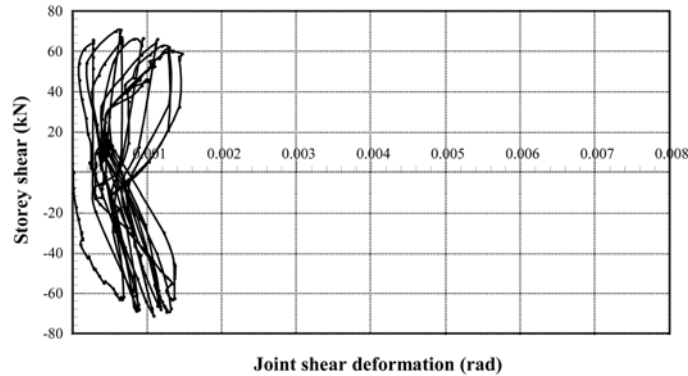


Fig. 9 Storey shear-joint shear deformation for the steel-reinforced specimen *J1*

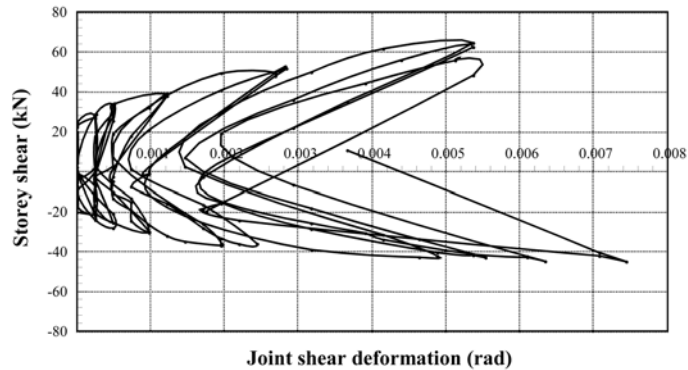


Fig. 10 Storey shear-joint shear deformation for the GFRP-RC specimen *J4*

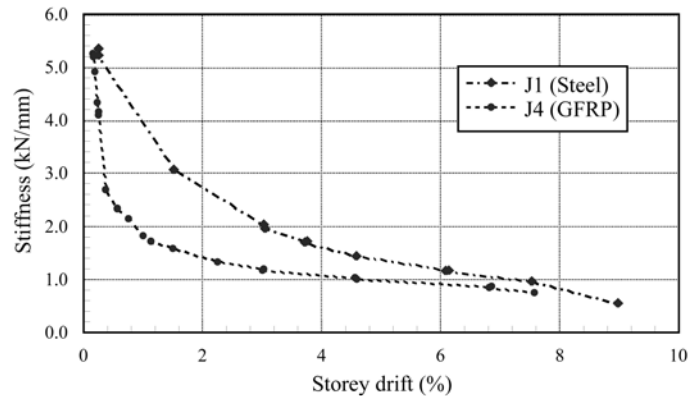


Fig. 11 Secant stiffness-storey drift for the tested specimens

reinforced frame that they tested exceeded the calculated values, which was attributed to joint panel deformations. However, since no joint panel deformation measurements were made in their test, this assumption which was not fully confirmed in their study is apparent in the results of the current study.

3.5. Secant stiffness relationship

Secant stiffness is evaluated as the peak-to-peak stiffness of the beam tip load-displacement relationship. Its value represents the specimens' damage through strength degradation from one cycle to the following cycle. Loss of stiffness of RC elements during cyclic loading is due several internal damage mechanisms (Priestly, *et al.* 1996). An examination of the secant stiffness plots for the tested beam-column joint specimens (Fig. 11) indicates that both specimens had comparable initial stiffness. Subsequently, after cracking the stiffness of the GFRP-RC specimen (*J4*) drops drastically. However, both specimens possess comparable stiffness at higher storey drifts. The GFRP-RC specimen (*J4*) had insignificant reduction in stiffness past 2% storey drift, which was attributed to the stabilization of cracks and the limited damage to concrete. In contrast, the steel-reinforced specimen (*J1*) had an almost continuous loss of stiffness associated with damage in the beam plastic hinge zone higher initial stiffness.

3.6. Cumulative dissipated energy

The capacity of a structure to survive an earthquake depends on its ability to dissipate the energy input. The energy dissipation of the specimens under cyclic loading is defined as the summation of the area enclosed by the load-displacement hysteretic loops. It can be observed from the energy dissipation plots (Fig. 12) that the standard RC specimen (*J1*) had about 4 times higher cumulative energy dissipation capacity at failure than that of the GFRP-RC specimen (*J4*). This is also clear from the shape of the individual hysteretic loops of the tested specimens (Figs. 4 and 6) which are much wider for the steel specimen compared to the GFRP-RC one due to its ductile behavior. The damage levels that the specimens sustained at failure, shown in Figs. 5 and 7, indicate that while for the steel-reinforced specimen extensive damage in the beam hinge area helped the specimen to dissipate energy, the GFRP-RC specimen sustained severe but localized damage.

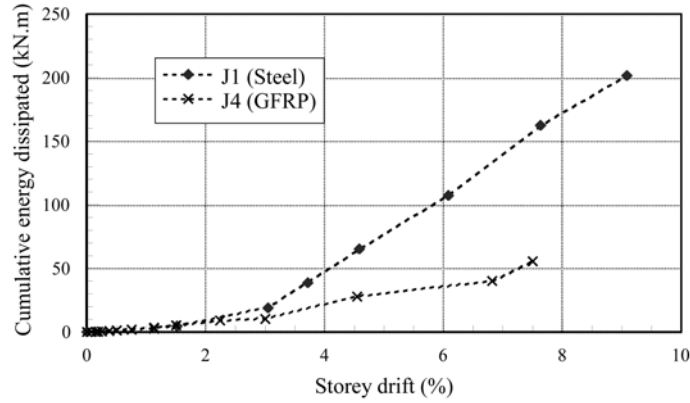


Fig. 12 Cumulative energy dissipated for the tested specimens

3.7. Beam moment-rotation relationship

Two LVDT's mounted on top and bottom of the beam were used to measure beam rotation of at 175 mm from the column. This area of the beam adjacent to the column is undergoes the majority of damage during cyclic loading. The rotation angle, θ , was calculated using the following expression:

$$\theta = \frac{(\delta_1 + \delta_2)}{d} \tag{3}$$

where δ_1 is the elongation on the tensile face of the beam, δ_2 is the shortening on the compressive face of the beam, and d is the vertical distance between the transducers. The beam rotation angle versus applied moment plots for the specimens (J1) and (J4) are shown in Figs. 13 and 14, respectively.

The plots show that specimen J1 had a significantly lower pre-yield rotations (at similar bending moments) compared to that of the beam in specimen J4. The lower stiffness of GFRP rebars caused higher rotations in the GFRP-RC beam at similar moments. However, the predominantly elastic behavior of GFRP resulted in very low residual deformations in the beam. The extent of damage in the beam for specimens (J1) and (J4) as shown in Figs. 5 and 7, respectively indicates less spalling in the

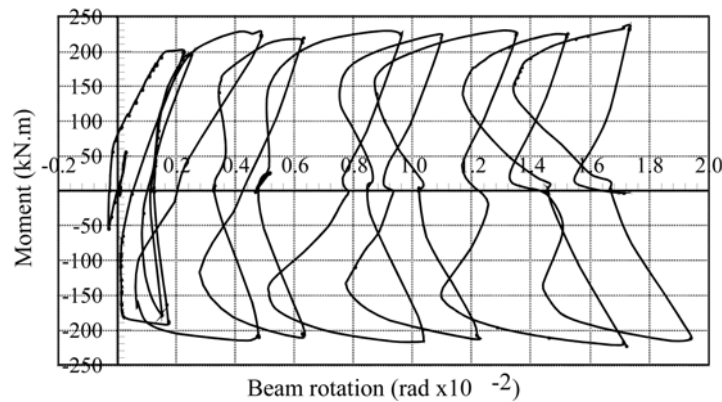


Fig. 13 Beam moment-rotation plot at 175 mm from the column face for the steel-reinforced specimen J1

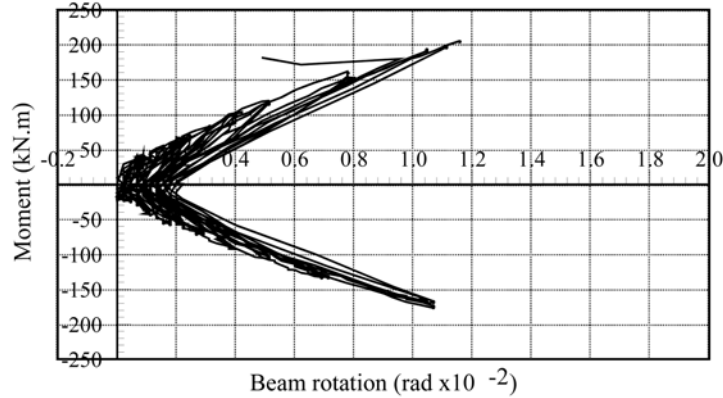


Fig. 14 Beam moment-rotation plot at 175 mm from the column face for the GFRP-RC specimen J4

beam of the GFRP-RC specimen despite the large number of cracks. Also, no GFRP stirrup failure was apparent in the GFRP-RC specimen, while extensive deformations in the steel stirrups were observed in the steel-reinforced specimen. This indicates that the amount of transverse reinforcement for the GFRP-RC specimen, which conformed to ACI 440.1R-06, was sufficient to prevent shear failure in the beams.

3.8. Damage index

The damage index, D , is a parameter that defines the extent of damage sustained by the specimen through the ratio of its stiffness at a specific cycle to its initial stiffness (Lemaitre and Desmorat 2005). It is calculated through the following equation:

$$D_n = 1 - \frac{E_n}{E_o} \tag{4}$$

where E_o and E_n are the original stiffness and the stiffness at the n^{th} cycle of the specimen, respectively.

Fig. 15 shows the GFRP-RC specimen having a larger damage index initially compared to the steel reinforced specimen. This is due to the fact that after cracking, the section loses the contribution of its cracked concrete part to stiffness. For FRP sections, this portion is high since the reinforcement

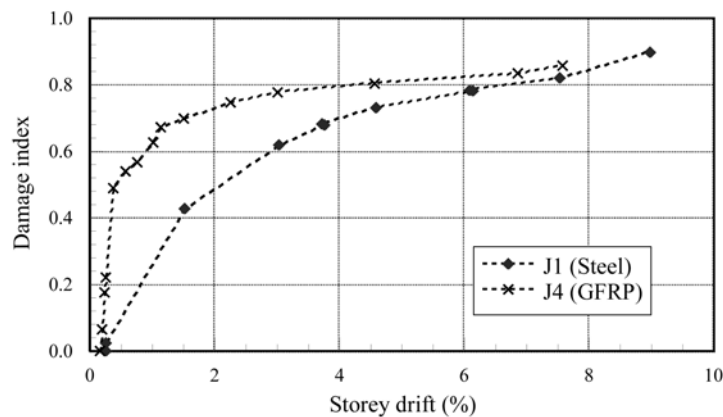


Fig. 15 Damage index-storey drift for the tested specimens

stiffness is lower than that of steel. Nonetheless, comparable values for the damage index are observed past the 4% drift.

4. Discussion

The use of FRP as reinforcement in concrete structures has been increasing in popularity, especially with the rising price of steel, yet various design guidelines and provisions still need to be further developed for its safe implementation in large-scale field applications as indicated by most of the existing standards. A major drawback of FRP-RC systems is their low energy dissipation under earthquake loading, as demonstrated by the performance of the tested FRP-reinforced joint specimen (*J4*). Accordingly, a FRP-RC frame may have to be designed with damping devices so that it can dissipate the energy input during an earthquake. Design guidelines for framed RC buildings by the AIJ, as outlined by Kobayashi, *et al.* (2003), entail ensuring seismic performance by overcoming the ductility deficiency of FRP-RC frames. The study concluded that FRP-RC structures may possibly be designed in seismic zones if the response is kept within the capacity of the FRP rebars.

5. Conclusions

The presented study investigated the damage characteristics of beam-column joints constructed using GFRP reinforcement compared to joints with conventional steel reinforcement under simulated earthquake loading. The GFRP-RC specimen exhibited very low plasticity resulting in lower energy dissipation compared to that of the steel-reinforced specimen. The elastic nature and low modulus of elasticity of the GFRP reinforcement distinctly defined its behavior with respect to the steel reinforced specimen in terms of deformation and damage. This also reflected on the manner both specimens failed. While the steel reinforced specimen underwent significant damage in the plastic hinge zone, the damage in the FRP-RC specimen was localized and very limited. Nonetheless, the GFRP-RC specimen's behavior is deemed satisfactory in terms of drift (Corley 1995).

References

- ACI Committee 440 (2006), *Guide for the Design and Construction of Concrete Reinforced with FRP Bars*, ACI 440.1R-06, ACI, Detroit.
- Alsayed, S.H., Al-Salloum, Y.A. and Almusallam, T.H. (1997), "Shear design of GFRP bars", *Proc. of 3rd Int. Sym. on Non-Metallic Reinforcement for Concrete Structures*, FRPRCS-3, Sapporo, Japan, 285-292.
- Canadian Highway Bridge Design Code (CHBDC) (1998), *Fibre reinforced structures*, Sec. 16, 687-705.
- Corley, W.G. (1995), "Ductility of columns, walls, and beams-how much is enough?", *Proc. of The Thomas Paulay Sym., Recent Developments in Lateral Force Transfer in Buildings*, ACI SP-157, 1993, 331-350.
- CSA A23.3-04 (2005), *Design of Concrete Structures*, Canadian Standards Association, Rexdale, Ontario, Canada.
- CSA S806-02 (2002), *Design and Construction of Building Components using Fibre-Reinforced Polymers*, Canadian Standards Association, Ontario, Canada.
- Dutta, P.K., Bailey, D.M., Tsai, S.W., Jensen, D.W., Hayes Jr., J.R., McDonald, W.E., Smart, C.W., Colwell, T., Earl, J.S. and Chen, H.J. (1998), "Composite grids for reinforcement of concrete structures", US Army Corps of Engineers, Construction Engineering Research Laboratories, USACERL Technical Report 98/81, 158 p.
- Fukuyama, H., Masuada, H., Sonobe, Y. and Tanigaki, M. (1995), "Structural performance of concrete frames

- reinforced with FRP reinforcement”, *Proc. of the 2nd Int. RILEM Sym. on Non-Metallic (FRP) Reinforcement for Concrete Structures*, FRPRCS-2, Ghent, Belgium, 275-286.
- ISIS Canada (2001), *Reinforcing Concrete Structures with Fibre Reinforced Polymers*, Manual No. 3.
- Joint ACI-ASCE Committee 352 (2002), *Recommendations for Design of Beam Column Connections in Monolithic Reinforced Concrete Structures*, ACI, Detroit.
- JSCE (1997), *Recommendations for the Design and Construction of Concrete Structures using Continuous Fiber Reinforcing Materials*, Concrete Eng. Series 23.
- Kobayashi, K., Fukuyama, H., Fujisaki, T., Fukai, S. and Kanakubo, T. (2003), “Design practice of framed building structures based on AIJ design guideline 2002”, *Proc. of the 6th Int. Sym. on Fiber Reinforced Polymers in Concrete Structures*, FRPRCS-6, Singapore, 1435-1444.
- Lemaitre, J. and Desmorat, R. (2005), *Engineering Damage Mechanics: Ductile, Creep, Fatigue and Brittle Failures*, Springer, The Netherlands.
- Nagasaka, T., Fukuyama, H. and Tanigaki, M. (1993), “Shear performance of concrete beams reinforced with FRP stirrups”, *Proc. of the Int. Sym. on Fiber Reinforced Plastic Reinforcement for Concrete Structures*, ACI SP-138, 789-811.
- NEFCOM Corporation (1996), *Mechanical Properties of NEFMAC*, Tokyo.
- Priestly, M.J.N., Seible, F. and Calvi, G.M. (1996), *Seismic Design and Retrofit of Bridges*, Wiley Interscience, New York.
- Rahman, A.H., Kingsley, C.Y. and Kobayashi, K. (2000), “Service and ultimate load behavior of bridge deck reinforced with carbon FRP grid”, *J. Compos. Constr.*, **4**(1), 16-23.
- Sharbatdar, M.K. and Saatcioglu, M. (2004), “Behaviour of FRP reinforced concrete under simulated seismic loading”, *Proc. of the 13th World Conf. on Earthquake Engineering*, Vancouver, Canada, Aug. 1-6, Paper No. 2717.
- Shehata, E.F.G (1999), “Fibre-Reinforced Polymer (FRP) for Shear Reinforcement in Concrete Structures”, Ph. D. Thesis, University of Manitoba, Canada.
- Sugita, M. (1993), *NEFMAC grid type reinforcement*, Alternative Materials for The Reinforcing and Prestressing of Concrete, Clarke, J. L. (Ed.), Blackie Academic and Professional, pp. 55-82.
- Uzumeri, S.M. and Seckin, M. (1974), “Behaviour of reinforced concrete beam-column joints subjected to slow load reversals”, Report No. 74-05, Department of Civil Engineering, University of Toronto, 72 p.